Biochimica et Biophysica Acta 1848 (2015) 95–103

Contents lists available at ScienceDirect

Biochimica et Biophysica Acta

journal homepage: www.elsevier.com/locate/bbamem

Synthesis, physicochemical characterization and membrane interactions of a homologous series of *N*-acylserotonins: Bioactive, endogenous conjugates of serotonin with fatty acids

S. Thirupathi Reddy, Musti J. Swamy *

School of Chemistry, University of Hyderabad, Hyderabad 500046, India

ARTICLE INFO

Article history:
Received 7 May 2014
Received in revised form 13 September 2014
Accepted 29 September 2014
Available online 5 October 2014

Keywords:
Differential scanning calorimetry
Phase transition
Odd–even alternation
Powder X-ray diffraction
Interdigitated bilayer

ABSTRACT

N-Acylserotonins (NASTs), present in the mammalian gastro-intestinal tract and central nervous tissues, exhibit significant biological and pharmacological activities. In the present study, a homologous series of NASTs have been synthesized and characterized. Differential scanning calorimetric studies show that in the dry and hydrated states the transition temperatures, enthalpies, and entropies of NASTs exhibit odd–even alternation. Both odd and even chain length NASTs independently display linear dependence of the transition enthalpies and entropies on the chain length under dry as well as hydrated conditions, suggesting that the molecular packing and intermolecular interactions in each series (odd or even) are likely to be similar for NASTs with different acyl chain lengths in the dry state as well as in the hydrated state. Powder X-ray diffraction studies indicated that the incremental increase in the *d*-spacing per CH_2 group is 1.023 Å, suggesting that the lipid acyl chains are most likely packed in an interdigitated fashion. Results of computational studies are consistent with this and suggest that the acyl chains of the NASTs are tilted with respect to the bilayer normal. Incorporation of *N*-myristoylserotonin (NMST) into dimyristoylphosphatidylcholine (DMPC) membranes did not significantly affect the phase transition properties at low mole fractions (1–5 mol%), although distinct decrease in the chain-melting transition temperature and increase in the pretransition temperature were observed at higher contents (7.5–30 mol%), suggesting that NMST increases the stability of the tilted gel phase ($L_{\beta'}$) but destabilizes the ripple phase ($P_{\beta'}$). These observations provide a thermodynamic basis for understanding the functional role of NASTs in their parent tissues.

1. Introduction

Although lipids—the main constituents of biomembranes—are simple amphiphilic molecules and do not adopt complex structures like proteins and nucleic acids, they form various supramolecular self assemblies in excess water. The type and size of such assemblies depend both on the structures of the lipids and other factors such as temperature, pH, and ionic strength. Although for long lipids have been considered as dull molecules as compared to proteins, which perform a variety of functions, e.g., catalysis, transport across membranes and immune recognition, and nucleic acids, which carry genetic information, in recent years, the conventional view of lipids has changed significantly and their role as second messengers in cell signaling, function, and health have been emphasized [1,2]. Recent reports suggest that perturbations in lipid pathways or lipid metabolism can lead to alterations in the numerous physiological and cellular processes, causing neurodegenerative disorders like Alzheimer's disease and cancer [3,4].

In keeping with the increased awareness of the functional roles of lipids in health and diseases, a new initiative, namely lipid metabolites and pathways strategy (LIPID MAPS) has been taken up to identify and quantify all the lipid species present in mammalian tissues. The goal of this is to quantify the changes in various species in response to perturbation and to characterize their biochemical and biophysical roles. One important class of lipids is fatty acid amides, which have been further categorized into various subclasses including *N*-acyl primary amines and *N*-acylethanolamines [5–7]. Fatty amides are present widely in the nature and act as signaling molecules in various physiological processes [8]. Among these, *N*-acylethanolamines (NAEs), which have been studied extensively so far due to their putative role in combating stress and interesting biological and medicinal properties [9–11].

More recently, much attention has been focused by the biomedical researchers on *N*-acyl conjugates of amino acids and neurotransmitters (NAANs) due to their potential roles in nervous system, vasculature, and the immune system [12]. Among NAANs, *N*-acylserotonins (NASTs), which are amides of long chain fatty acids with serotonin have been found to be present in the gut of mammals [13]. Serotonin, an endogenous molecule that acts as a neurotransmitter, is widely distributed in

* Corresponding author. Tel.: +91 40 2313 4807; fax: +91 40 2301 2460.
E-mail addresses: mjssc@uohyd.ernet.in, mjswamy1@gmail.com (M.J. Swamy).

http://dx.doi.org/10.1016/j.bbamem.2014.09.012
0005-2736/

the central and peripheral nervous system, as well as other parts of the body [14]. Serotonin exerts its diverse actions by binding to specific cell surface receptors such as the serotonin$_{1A}$ receptor, an extensively studied member of G-protein coupled receptor family, which plays a key role in serotonergic signaling [15,16]. Due to the high abundance of serotonin in the intestine, and central nervous system (CNS) [17–20], it may be speculated that *N*-acylserotonins would be formed in the gastrointestinal tissues and in the CNS. Recently, the presence of several different *N*-acylserotonins bearing saturated as well as unsaturated fatty acyl chains was reported in the gastrointestinal tract of pig and mice [13] and it may be expected that similar investigations on neuronal tissues of mammals would lead to the identification of NASTs in the CNS as well.

Among the NASTs, *N*-arachidonylserotonin (NArST) has been reported to function as a *dual blocker* of endocannabinoid-inactivating enzyme, fatty acid amide hydrolase (FAAH) and a transient receptor potential vanilloid type 1 (TRPV1) receptor antagonist [21,22]. NArST was also shown to decrease anxiety-like behavior of mice in the elevated plus maze (EPM) when administered systemically. Furthermore, NArST alone is highly effective at reducing anxiety than selective blockers of FAAH or TRPV1 channels [23]. NArST also increases anxiolytic behavior in the EPM of basolateral amygdala, a major limbic-related region of the brain [24]. Since analysis of lipid extracts from different parts of the gastrointestinal tract of pig and mice has also shown the presence of saturated *N*-acylserotonins [13], it is likely that *N*-acylserotonins bearing saturated acyl chains would be present in the gastrointestinal tracts of other animals as well in other parts of the body.

From the foregoing, it is clear that *N*-acylserotonins are a new group of endogenous molecules, with interesting biochemical and pharmacological activities. In view of this, it is important to investigate their physicochemical characteristics and membrane interactions. In the present study we synthesized and characterized a homologous series of saturated *N*-acylserotonins with varying acyl chain lengths ($n = 11$–20) by differential scanning calorimetry (DSC), powder X-ray diffraction (PXRD) and computational modeling and investigated the interaction of *N*-myristoylserotonin with dimyristoylphosphatidylcholine by DSC.

2. Materials and methods

2.1. Materials

Fatty acids were purchased from Sigma-Aldrich (Milwaukee, WI). Serotonin hydrochloride was purchased from Tokyo Chemical Industry (Tokyo, Japan). 1-Hydroxybenzotriazole (HOBT), 1-ethyl-3(3-dimethylaminopropyl)carbodiimide (EDC) and triethylamine were obtained from Merck (Germany). Dimyristoyl phosphatidylcholine (DMPC) was purchased from Avanti Polar Lipids (Alabaster, AL) Solvents and other chemicals used were of analytical grade and purchased locally. Milli-Q water was used in all experiments.

2.2. Synthesis of N-acylserotonins

N-Acylserotonins were synthesized by a simple condensation reaction between fatty acids and serotonin using a reported procedure [25] with minor modifications (Scheme 1). Briefly, to a stirred solution of fatty acid (1 eq.) at 0 °C in DMF, HOBT (1 eq.) and EDC (1 eq.) were added and stirred for 15 min at 0 °C, brought to room temperature and allowed to stand for 1 h. Serotonin hydrochloride (1.2 eq.) and triethylamine (1.5 eq.) were added to the reaction mixture and the reaction vessel was kept under stirring overnight at room temperature. The mixture was then washed with brine and extracted with ethyl acetate. The organic solution was washed successively with 2 N HCl, saturated sodium bicarbonate, brine, and twice with Milli-Q water, dried over anhydrous sodium sulfate and evaporated using

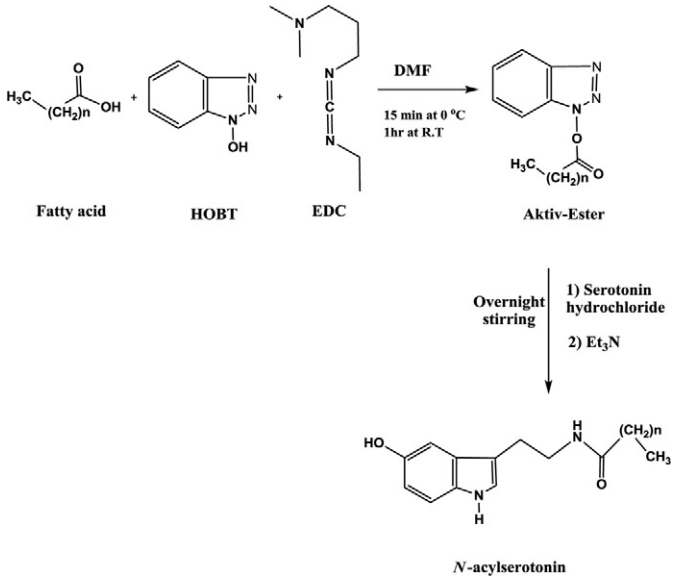

Scheme 1. Synthesis of *N*-acylserotonins.

rotary evaporator under reduced pressure. The crude product was purified on a silica gel column by using increasing concentrations of ethyl acetate in dichloromethane (DCM) and recrystallized twice from DCM at −20 °C. Overall yields of NASTs thus obtained were around 60–65%. The purified compounds were characterized by TLC, melting point, FTIR, ^{1}H- and ^{13}C-NMR spectroscopy, and high resolution mass spectrometry.

Capillary melting points of the NASTs were recorded on a Superfit (Mumbai, India) melting point apparatus [26]. IR spectra were recorded using KBr pellet on a Thermo Scientific NICOLET 380 FT-IR spectrometer and ^{1}H-NMR spectra were recorded in $CDCl_3$ on a Bruker Avance NMR spectrometer at 400 MHz, whereas ^{13}C-NMR spectra were recorded at room temperature in CD_3OD at 100 MHz on the same spectrometer. Mass spectra of NASTs were obtained in the positive ion mode on a Bruker Maxis high-resolution mass spectrometer equipped with electrospray ionization system.

2.3. Differential scanning calorimetry

The thermotropic phase transitions of dry NASTs were investigated by differential scanning calorimetry on a Perkin-Elmer PYRIS Diamond differential scanning calorimeter. Dry powdered samples of individual NASTs (1–2 mg) were weighed accurately into aluminium sample pans, covered with an aluminium lid and sealed by crimping. Reference pans were prepared similarly but without any sample in them. Heating and cooling scans were performed from room temperature (ca. 25 °C) to about 140 °C at a scan rate of 1.5°/min and each sample was subjected to three heating scans and two cooling scans. Transition enthalpies were determined by integrating the area under the transition curves. Transition entropies were calculated from the transition enthalpies assuming a first order phase transition according to the expression [27]:

$$\Delta H_t = T_t \Delta S_t \quad (1)$$

where T_t is the transition temperature and ΔH_t values corresponding to the transition at this temperature were used to calculate the corresponding ΔS_t values.

DSC studies on hydrated NASTs were carried out on a VP-DSC microcalorimeter from MicroCal (Northampton, MA). Accurately weighed NASTs (3–4 mg) in clean, dried glass test tubes were dissolved in about 300 μL of dichloromethane containing a few drops of methanol.

A thin film of the lipid was obtained on the inner walls of the tube by passing a gentle stream of dry nitrogen gas. Final traces of solvent were removed by applying high vacuum desiccation for 3–4 h. Then the sample was hydrated by adding 1.0 mL double distilled water to the thin film, followed by vigorous vortexing and then heating to about 50 °C in a hot water bath. The hydrated lipid suspension was then subjected to about 5 cycles of freeze–thawing with intermittent vortexing. The resulting homogeneous dispersion was used for the DSC studies. All the samples were subjected to three heating and two cooling scans from 10 °C to 125 °C at a scan rate of 1 °/min. In each case, only the first heating scan was considered for the further analysis. Transition enthalpies were calculated by integrating the area under the transition curve after blank (water) subtraction, normalization and baseline correction. Transition entropies were determined from the transition enthalpies by using Eq. (1).

2.4. Powder X-ray diffraction

Powder X-ray diffraction patterns of *N*-acylserotonins were recorded on a SMART Bruker D8 Advance X-ray diffractometer (Bruker-AXS, Karlsruhe, Germany) using Cu–K_α radiation ($\lambda = 1.5406$ Å) at 40 kV and 30 mA at 25 °C. Samples were placed and pressed on a circular rotating disk of the sample holder. The diffracted beam from the sample was detected by a LynxEye PSD data collector. Diffraction patterns were collected for all the NASTs at room temperature over a 2θ range of 2–50° with a step size of 0.0198°, with a measuring time of 10 s for each step. The compounds were ground with the help of a pestle and mortar, and the homogenous powder obtained was used for PXRD measurements.

2.5. Computational studies

The geometry of *N*-acylserotonins was optimized in their ground state using DFT based B3LYP (Beckye Lee Yang-Paar) functional and 6-311G basis set using Gaussian g03 software [28]. The stationary state is confirmed by doing vibrational mode frequency calculations. All the vibrational frequencies obtained from all the calculations are real. The polymorphs of these molecules were obtained by using Materials Studio 6.0 program package [29].

3. Results and discussion

3.1. Synthesis and characterization of N-acylserotonins

A homologous series of *N*-acylserotonins have been synthesized in the present study by a simple condensation of serotonin with fatty acids containing saturated acyl chains (n = 11–20 C atoms). The structure and purity of the synthesized NASTs were characterized by TLC and FTIR, ^{1}H NMR, and ^{13}C NMR spectroscopy as well as by high resolution mass spectrometry. Representative FTIR and ^{1}H NMR spectra of *N*-lauroylserotonin (NLST) are given in Fig. S1 and Fig. S2, respectively. FTIR spectra (KBr pellet) of freshly prepared NASTs showed absorption bands due to amide linkage at 1644–1632 cm^{-1} (amide-I) and 1545–1534 cm^{-1} (amide-II), whereas the amide N–H stretching band was seen at 3315–3298 cm^{-1}. The O–H, N–H, and C–H stretching bands of the 5-hydroxy indole moiety were observed around 3501–3496 cm^{-1}, 3414–3408 cm^{-1}, and 3063–3057 cm^{-1}, respectively. The stretching, bending, and rocking modes of the polymethylene portion of the hydrophobic acyl chain were seen at 2926–2838 cm^{-1}, 1479–1462 cm^{-1}, and 723–707 cm^{-1}, respectively. The FTIR data for all the NASTs are summarized in Table S1. The ^{1}H NMR spectra of NASTs showed resonances at 2.30–2.14 δ (2H, t) and 1.62–1.55 δ (2H, m) for the methylene groups at α and β positions to the carbonyl moiety, at 6.68–5.73 δ (1H, bs) for the amide N–H, at 3.61–3.49 δ (2H, q) for the methylene group at the α position to the amide N–H, and at 3.04–2.84 δ (2H, t) for the methylene group connected to the aromatic ring. The hydroxy group gave a broad singlet at 8.15–7.92 δ (1H, bs), whereas the aromatic proton resonances were seen between 7.27 and 6.77 δ. The resonances of terminal methyl was seen at 0.94–0.89 δ (3H, t), whereas the polymethylene part of the acyl chain yielded an intense signal at 1.29–1.22 δ (14–32H, m). These ^{1}H NMR data for all the NASTs are listed in Table S2.

A representative ^{13}C NMR spectrum of NLST is given in Fig. S3. The terminal methyl resonance is seen at 13.08 δ and resonances corresponding to the methylene groups of the acyl chain as well as the serotonin moiety are seen at 22.35, 24.96, 25.69, 31.69, 35.84, and 39.85 δ and as well as 5 peaks between 28.90 and 29.35 δ (the peak at 29.35 δ being more intense than the others). Eight peaks observed between 102.22 and 149.80 δ correspond to the aromatic carbons. The carbonyl resonance is seen at 174.99 δ. These values are consistent with the structure of *N*-lauroylserotonin. The ^{13}C-NMR spectra of all other NASTs were very similar, except that the intensity of the peak at ~29.35 δ increased with increase in the acyl chain length.

A high-resolution ESI mass spectrum of NLST is shown in Fig. S4. The most intense peak seen at 359.2699 matches well with the molecular ion of the compound ($[M + H]^+$, calc. mass 359.2698). In addition, prominent peaks are also seen at 381.2519 ($[M + Na]^+$, calc. mass 381.2518), 717.5316 ($[M_2 + H]^+$, calc. mass 717.5319), 739.5139 ($[M_2 + Na]+$, calc. mass 739.5138), 1075.7863 ($[M_3 + H]^+$, calc. mass 1075.7939) and 1097.7693 ($[M_3 + Na]^+$, calc. mass 1097.7758), which correspond to proton and sodium adducts of monomer, dimer and trimer of NLST as indicated in the parentheses. For both proton adducts and sodium ion adducts, the intensity of the peaks decreases with increasing size of the adducts. While for the monomer the proton adduct is more intense, the sodium ion adduct was found to be more intense than the proton adduct for the dimer and trimer. Other NASTs also yielded essentially similar mass spectra. These data are given in Table S4.

The above results from FTIR, ^{1}H- and ^{13}C-NMR spectroscopy as well as ESI mass spectrometry are fully consistent with the structures of *N*-acylserotonins and indicate that they are of high purity.

3.2. Differential scanning calorimetry

Heating thermograms corresponding to dry NASTs of odd acyl chain lengths are presented in Fig. 1A and those corresponding to the even chain length series are shown in Fig. 1B. The thermograms show that each NAST exhibits a major endothermic transition, which corresponds to the capillary melting point of the compound (Table 1 & Table S5).

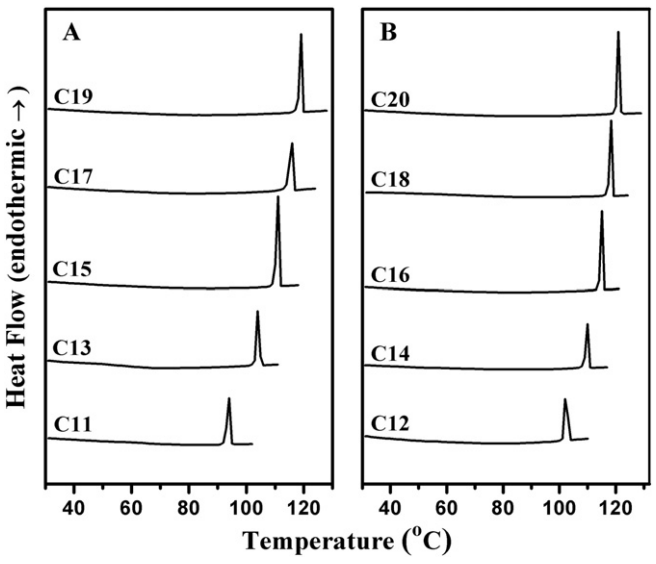

Fig. 1. DSC heating thermograms of dry NASTs with (A) odd and (B) even acyl chain lengths. The number of C-atoms in the acyl chain is indicated against each thermogram.

Table 1
Average values of transition temperatures (T_t), transition enthalpies (ΔH_t), and transition entropies (ΔS_t) of NASTs in dry and hydrated states.

Acyl chain length	Dry NASTs			Hydrated NASTs		
	T (°C)	ΔH_t (kcal/mol)	ΔS_t (cal/mol/K)	T (°C)	ΔH_t (kcal/mol)	ΔS_t (cal/mol/K)
11	93.9 ± 0.1	08.90 ± 0.03	24.3 ± 0.1	80.8 ± 0.1	3.13 ± 0.29	8.85 ± 0.8
12	102.6 ± 0.1	10.67 ± 0.05	28.4 ± 0.1	90.4 ± 0.1	6.92 ± 0.82	19.04 ± 2.3
13	104.4 ± 0.1	10.84 ± 0.01	28.7 ± 0.1	92.3 ± 0.1	5.39 ± 0.84	14.75 ± 2.3
14	110.2 ± 0.1	12.33 ± 0.02	32.2 ± 0.1	98.9 ± 0.1	8.46 ± 1.04	22.75 ± 2.9
15	110.9 ± 0.1	12.38 ± 0.01	32.3 ± 0.1	99.8 ± 0.1	7.78 ± 0.68	20.87 ± 1.9
16	115.1 ± 0.2	14.08 ± 0.11	36.3 ± 0.3	104.3 ± 0.1	10.64 ± 1.74	28.20 ± 3.8
17	115.7 ± 0.1	14.17 ± 0.11	36.5 ± 0.3	105.3 ± 0.1	09.34 ± 0.75	24.69 ± 1.9
18	118.4 ± 0.1	15.39 ± 0.02	39.3 ± 0.1	108.4 ± 0.1	11.81 ± 2.65	30.97 ± 5.7
19	118.9 ± 0.1	15.88 ± 0.20	40.5 ± 0.5	108.9 ± 0.1	10.96 ± 2.49	28.69 ± 3.3
20	121.1 ± 0.1	17.42 ± 0.14	44.2 ± 0.4	111.3 ± 0.1	13.63 ± 1.99	35.47 ± 4.4

When the samples were subjected to a second heating scan, in some cases the thermograms became more complex, involving multiple transitions (Fig. S5), which at least in some cases, could be due to partial degradation of the samples when subjected to heating to high temperatures. It is also possible, especially for the shorter chain length NASTs—which did not show reversal of the heating transition upon cooling (not shown)—that they go into a metastable, liquid crystalline state. Therefore in all the cases only the first heating scan was considered for further analysis and the transition temperatures, enthalpies and entropies obtained are presented in Table 1.

Heating thermograms of hydrated NASTs with odd and even chain lengths are shown in Fig. 2A and B, respectively. Each thermogram exhibits a single, sharp phase transition. When the samples were subjected to a second heating scan, a minor (exothermic) transition was observed at a lower temperature as compared to the main phase transition (Fig. S6). Additionally, enthalpy of the main transition decreased slightly in the second and subsequent scans. Interestingly, the hydrated NASTs were highly turbid before loading in the DSC sample cell, whereas after the heating and cooling scans, the sample solutions recovered from the DSC cell were optically clear, and remained so for several days. The phase transition temperatures (T_t), transition enthalpies (ΔH_t), and transition entropies (ΔS_t) determined from the DSC thermograms are listed in Table 1.

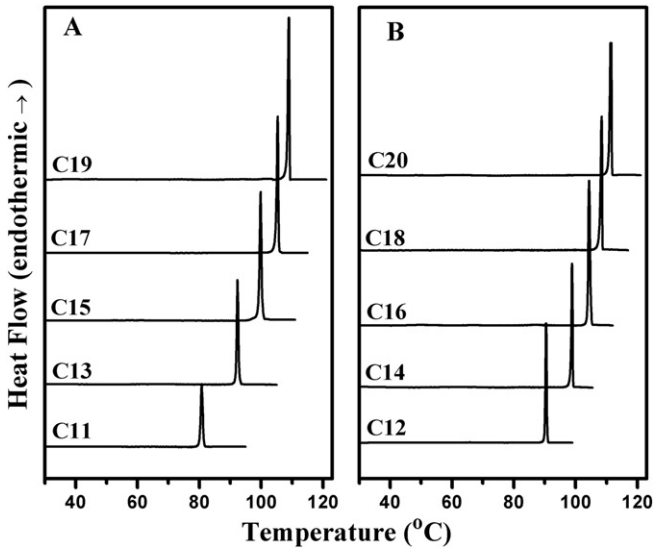

Fig. 2. DSC heating thermograms of hydrated NASTs with (A) odd and (B) even acyl chain lengths. The number of C-atoms in the acyl chain is indicated against each thermogram.

3.3. Chain length dependence and odd–even alternation in transition enthalpy and transition entropy

Chain length dependences of transition enthalpy and transition entropy for the chain-melting phase transitions of dry NASTs are given in Fig. 3A and B, respectively. In both cases, NASTs with odd and even acyl chains independently exhibit linear dependence of ΔH_t and ΔS_t on the acyl chain length. However, when the data obtained with odd and even acyl chain lengths are viewed together, a zig-zag pattern is seen with the values of enthalpy and entropy for the odd acyl chain lengths being slightly lower than those of even acyl chain lengths. That is, the calorimetric parameters exhibit odd–even alternation (discussed in more detail below). The transition enthalpies and entropies of dry NASTs with odd and even acyl chain lengths could independently be fit well to the following linear expressions [30]:

$$\Delta H_t = \Delta H_o + (n-2)H_{inc} \quad (2)$$

$$\Delta S_t = \Delta S_o + (n-2)\Delta S_{inc} \quad (3)$$

where n is the number of C-atoms in the acyl chain and ΔH_o and ΔS_o are the end contributions to ΔH_t and ΔS_t, respectively, arising from the terminal methyl group and polar region of *N*-acylserotonin molecule.

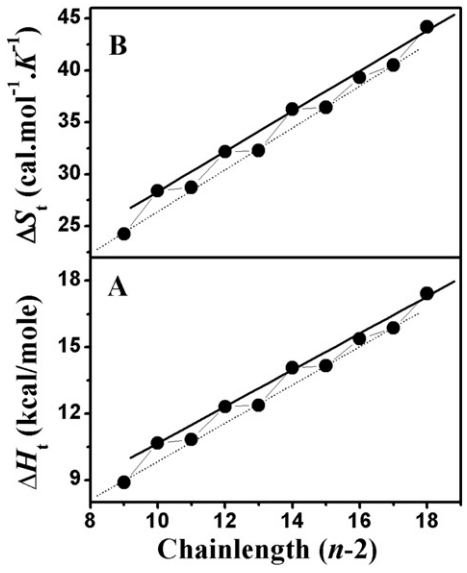

Fig. 3. Chain length dependence of transition enthalpies (A) and transition entropies (B) of dry NASTs. Values of ΔH_t and ΔS_t were plotted against the number of methylene (CH_2) units ($n-2$) in the acyl chains. Solid and dotted lines represent linear least squares fit of the data for even- and odd-chain length series, respectively.

Table 2
Incremental values (ΔH_{inc}, ΔS_{inc}) of chain length dependence and end contributions (ΔH_o, ΔS_o) to phase transition enthalpy and entropy of NASTs. Average values of transition enthalpy and transition entropy given in Table 1 have been used for the linear fitting of the data. Errors shown in parentheses are fitting errors obtained from the linear least squares analysis.

Sample	ΔH_{inc} (kcal/mol)	ΔH_o (kcal/mol)	ΔS_{inc} (cal/mol/K)	ΔS_o (cal/mol/K)
Dry NASTs (odd)	0.86 (±0.02)	−0.53 (±0.23)	2.01 (±0.03)	2.27 (±0.53)
Dry NASTs (even)	0.83 (±0.03)	0.74 (±0.43)	1.93 (±0.07)	5.13 (±1.15)
Hydrated NASTs (odd)	0.98 (±0.06)	−7.39 (±0.84)	2.48 (±0.16)	−17.65 (±2.42)
Hydrated NASTs (even)	0.84 (±0.04)	−3.12 (±0.61)	2.05 (±0.10)	−5.578 (±1.63)

ΔH_{inc} and ΔS_{inc} are the average incremental values contributed by each CH_2 group to ΔH_t and ΔS_t, respectively. From the least squares analysis, the values of ΔH_{inc} and ΔS_{inc} for NASTs with odd acyl chain lengths were obtained as 0.86 ± 0.02 kcal/mol and 2.01 ± 0.03 cal/mol/K, respectively, whereas the corresponding values for NASTs with even acyl chain lengths were obtained as 0.83 ± 0.03 kcal/mol and 1.93 ± 0.07 cal/mol/K, respectively. These values are given in Table 2. The linearity of chain length dependence of the thermodynamic properties associated with the phase transition, observed here, indicates that structures of the NASTs of different even chain lengths are very similar in the solid state. Similarly, the data also suggest that the structures of NASTs with odd acyl chain lengths would be very similar.

Chain length dependences of transition enthalpy and transition entropy for the thermotropic phase transitions of hydrated NASTs are shown in Fig. 4A and B, respectively. Similar to the dry NASTs, hydrated samples also show an odd–even alternation and the values of ΔH_t and ΔS_t for NASTs with odd and even acyl chain length series could be fitted individually to straight lines. From the linear least squares analysis, the incremental values and end contributions of transition enthalpy and entropy were obtained. These values are also listed in Table 2. It was observed that similar to dry NASTs, the structures of odd and even chain length NASTs within each series are very similar in the hydrated state. The values of ΔH_{inc} and ΔS_{inc} for odd and even chain length NASTs are 0.98 ± 0.06 kcal/mol and 2.48 ± 0.16 cal/mol/K, and 0.84 ± 0.04 kcal/mol and 2.05 ± 0.10 cal/mol/K, respectively.

3.4. Odd–even alternation in the thermodynamic properties

The odd–even alternation seen in the transition enthalpies, transition entropies and transition temperatures of NASTs is similar to the alternation observed previously in the thermodynamic properties of a number of other amphiphilic molecules such as long-chain hydrocarbons, fatty acids, *N*-acylethanolamines, *N*-, *O*-diacylethanolamines with matched as well as mixed chains, and *N*-acyldopamines in the solid state [26,30–34]. This could be explained on the basis of differences in the packing of hydrocarbon chains. For example, in long chain fatty acids, differences in the packing properties between the terminal methyl groups between the even and odd acyl chain lengths were used to explain the differences in the physical properties [30]. Such differences do not arise in the methyl group packing if the chains are perpendicular to the methyl group plane. However, if the hydrocarbon chains are tilted with respect to the plane of the methyl groups, their packing modes can differ, leading to alternation in the physical properties [30]. The above observations suggested that differences in the acyl chain packing and tilt might be responsible for the odd–even alternation in the thermodynamic properties of dry as well as hydrated NASTs.

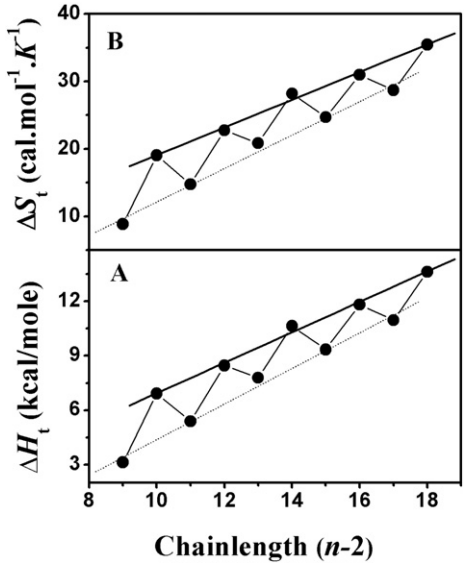

Fig. 4. Chain length dependence of transition enthalpies (A) and transition entropies (B) of hydrated NASTs. Values of ΔH_t and ΔS_t were plotted against the number of methylene (CH_2) units ($n-2$) in the acyl chains. Solid and dotted lines represent linear least squares fit of the data for even- and odd-chain length series, respectively.

3.5. Incremental values and end contributions of transition enthalpy and entropy

As indicated above, linear least squares analysis of transition enthalpies and entropies of dry and hydrated NASTs yielded values of ΔH_o and ΔS_o (end contributions) as well as ΔH_{inc} and ΔS_{inc} (incremental values) for the two cases. From Table 2, it is observed that ΔH_{inc} in the dry state for odd acyl chain lengths is distinctly lower than the ΔH_{inc} in the hydrated state. Since ΔH_{inc} gives a measure of cohesiveness of the acyl chain packing, these data indicate that the acyl chains in NASTs with odd chain lengths are packed more tightly in the hydrated state than in the dry state. Similar observations were made in the case of *N*-acyldopamines (NADAs) [26]. However, for NASTs with even acyl chain lengths the ΔH_{inc} values are comparable for both dry and hydrated samples, indicating similar chain packing under both conditions. The significantly higher value of ΔH_{inc} in the hydrated state of *N*-acyldopamines (NADAs) was explained on the basis of hydrophobic effect and π-stacking interactions. Higher ΔH_{inc} in NASTs with odd acyl chain lengths in the hydrated state as compared to the dry samples possibly arises from the hydrophobic effect and π-stacking of the aromatic rings of the indole moiety. Although the crystal structure of *N*-lauroyldopamine (NLDA) showed that the catechol moieties in adjacent layers are laterally displaced, resulting in a lack of π-stacking interaction of the aromatic rings in the solid state, it was suggested that in the hydrated state the NLDA molecules may be oriented in a different manner which allows π-stacking interactions [26]. The present results suggest that similar explanation may account for the higher value of ΔH_{inc} in the hydrated state for NASTs with odd acyl chain lengths. The end contribution of entropy, ΔS_o is also more negative for hydrated samples, especially for the odd chain length series, as compared to the dry state. The negative ΔS_o is also indicative of the hydrophobic effect playing a role in the acyl chain packing of NASTs, which could arise due to the ordering of water molecules around the indole moiety of the head group [35]. Together, these observations suggest that the hydrophobic effect and possibly π-stacking in the hydrated state bring the odd chain length NASTs closer, which results in a more compact packing of the acyl chains.

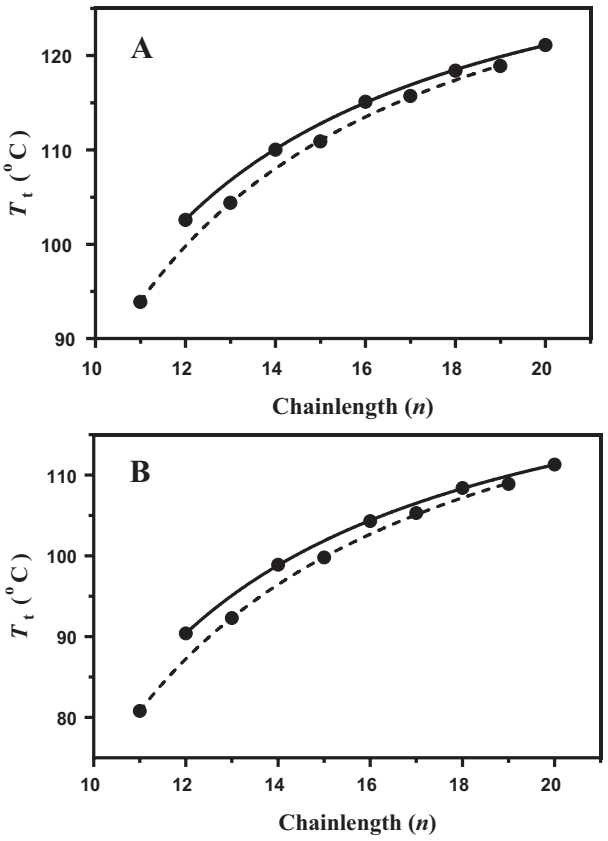

Fig. 5. Chain length dependence of phase transition temperatures of NASTs in the dry (A) and hydrated (B) states. Solid and dotted lines correspond to non-linear squares fits of transition temperatures of even- and odd-chain length series to Eq. (7). See text for details.

3.6. Chain length dependence of transition temperatures

From the DSC thermograms presented in Figs. 1 and 2 it can be seen that the transition temperatures of both dry and hydrated NASTs with even as well as odd acyl chains increase with increasing chain length. However, in both cases magnitude of the change decreases with increase in the chain length. Interestingly, for both dry and hydrated NASTs an alternation is seen between the odd-chain length and even-chain length series, with the even chain length series exhibiting slightly higher transition temperatures than the odd chain length compounds (Fig. 5A and B). With the dry and hydrated samples, for both odd and even chain length series, the T_t values increase in a smooth progression but with decreasing increments as the chain length is increased. As the acyl chain length increases, the total contribution from the polymethylene portion towards the total enthalpy and entropy of the phase transition will become sufficiently large, and the end contributions would be negligible in comparison. Therefore, at infinite acyl chain length, Eqs. (2) and (3) can be reduced to [30]:

$$\Delta H_t = (n-2)\Delta H_{inc} \quad (4)$$

$$\Delta S_t = (n-2)\Delta S_{inc} \quad (5)$$

Then the transition temperature for infinite chain length, T_t^{∞}, will be given by:

$$T_t^{\infty} = \Delta H_{inc}/\Delta S_{inc} \quad (6)$$

From the data presented in Table 2, the T_t^{∞} values for NASTs of odd and even acyl chain lengths in the dry state have been estimated using Eq. (6) as 427.9 and 430.1 K, respectively. Similarly in the hydrated state the T_t^{∞} values for odd and even chain-length NASTs were estimated as 395.2 and 409.8 K, respectively.

For a number of diacyl lipids as well as single chain amphiphiles, which exhibit linear dependence of transition enthalpy and transition entropy on chain length, it has been shown that the data can be fit to the following equation [31,32,36]:

$$T_t = \Delta H_t/\Delta S_t = T_t^{\infty}\left[1-(n_o-n'_o)/(n-n'_o)\right] \quad (7)$$

where $n_o(=-\Delta H_o/\Delta H_{inc})$ and $n'_o(=-\Delta S_o/\Delta S_{inc})$ are the values of n at which the transition enthalpy and transition entropy extrapolate to zero. It can be seen from Fig. 5A and B that the transition temperatures of dry and hydrated NASTs with odd as well as even number of C-atoms in the acyl chains independently fit quite well with Eq. (7). Additionally, the fitting parameters also yielded the T_t^{∞} values for odd and even chain length NASTs in the dry state as 413.7 K and 411.8 K, and in the hydrated state as 408.1 K and 404.7 K, respectively. These values are in reasonable agreement with the T_t^{∞} values estimated using Eq. (6).

3.7. Powder X-ray diffraction studies

Since our efforts to grow single crystals of the different NASTs did not succeed, in order to derive information on the structure adopted by them, we carried out powder X-ray diffraction studies. PXRD data obtained at room temperature (ca. 25 °C) for the various NASTs are shown in Fig. 6A and B. All the NASTs yielded diffraction patterns that are consistent with lamellar packing. For shorter chain length NASTs ($n = 11$–15), diffraction peaks were seen for n = 1–4 (Fig. 6A), whereas for longer chain length compounds diffraction peaks corresponding to n = 2–5 could be assigned (Fig. 6B). The d-spacings were estimated for each and the average values obtained are given in Table 3. The d-spacings exhibit a linear chain length dependence (Fig. 6C), suggesting that all the NASTs in the chain length range 11–20 are organized in a lamellar structure and have similar packing arrangement. The slope of the linear fit yielded an incremental value of 1.023 Å per methylene unit. It may be noted that increasing the chain length by one CH_2 unit would be expected to increase the d-spacing by about 2.54 Å for a regular lamellar bilayer structure as the projected length of the C–C single bond is 1.27 Å for untilted packing of lipid chains [37]. This value will be somewhat lower if the chains are tilted. However, the value of 1.023 Å obtained here for the incremental increase in the d-spacing corresponding to each additional methylene group in the acyl chain is significantly lower and hence suggests that the acyl chains are packed in an interdigitated fashion. If the interdigitated chains are in perfect register, then the incremental increase in d-spacing would be 1.27 Å, which will decrease if the chains are both interdigitated and tilted. From the value of 1.023 Å for the increase in d-spacing per CH_2 group, the angle of tilt of the chains with respect to the bilayer normal was estimated as 36.3°.

3.8. Computational studies on the molecular packing of NASTs

Since no crystal structure of NAST molecules was available in the literature, in order to investigate the structure and molecular packing of NASTs in crystalline state, we developed a molecular model for the NASTs using the reported crystal structure of *N*-lauroyldopamine [26], which bears considerable similarity to the structure of *N*-lauroylserotonin. NLDA was modified to *N*-acylserotonins with varying acyl chain lengths (n = 11 to 14) and the corresponding structures were obtained from the Gaussian energy minimization method as described above. The polymorphism for these molecules was calculated using Material Studio 6 (MS 6) to generate plausible packing arrangements for NASTs in the crystalline state. In order to

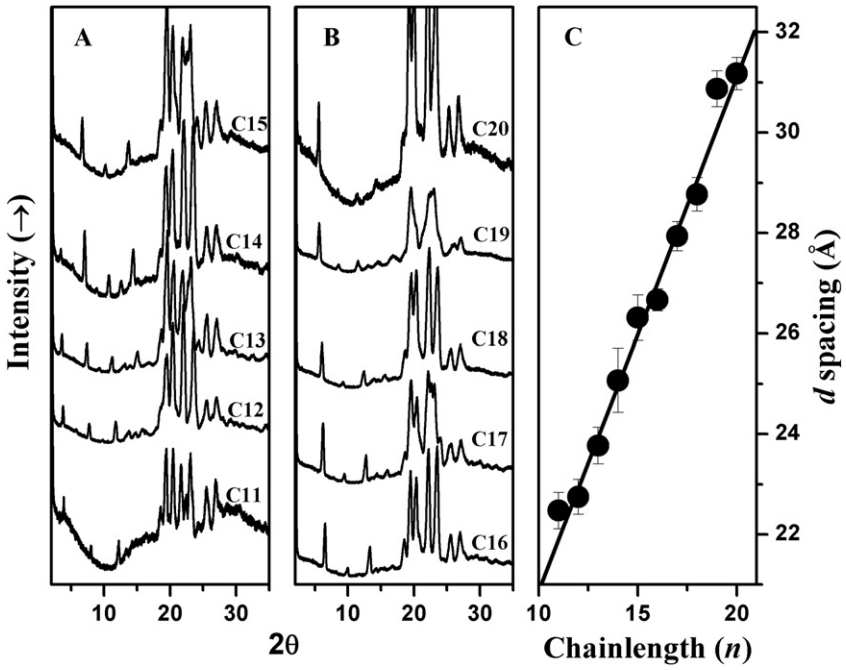

Fig. 6. Powder X-ray diffraction patterns of NASTs. Data are shown for compounds with acyl chains containing: (A) 11 to 15 C-atoms and (B) 16 to 20 C-atoms. The number of C-atoms in the acyl chain is indicated against each diffraction pattern. (C) Chain length dependence of *d*-spacing values for the NASTs. Solid line corresponds to linear least squares fit of the *d*-spacings.

investigate the packing arrangements in NASTs with different acyl chains we carried out computational studies on the bilayer packing of four NAST molecules ($n = 11$ to 14).

In the minimum energy structures of NASTs obtained by computational modeling, all the methylene groups in the hydrophobic region are in *trans* conformation, with all the torsion angles corresponding to the acyl region being in the neighborhood of 180°. In addition, all the atoms in the serotonin moiety of the head group are in the same plane. The angle between serotonin moiety and acyl chain was found to vary in the range of 102–129° for different NASTs, resulting in a bend in the molecule. Interestingly, the carbonyl oxygen and amide N–H are in *cis* geometry for all the four NASTs. A packing diagram of NLST obtained from the computational studies is shown in Fig. 7, as a representative example. From this figure it is clear that in the crystalline state, NLST molecules are most likely packed in an interdigitated bilayer fashion. The thickness of the (interdigitated) bilayer shown in Fig. 7 was 25.9 Å, which is in good agreement with the value of 22.8 (±0.4) Å estimated from the PXRD measurements. Similar packing arrangement was also seen in the minimum energy structures of the other NASTs whose molecular packing arrangements were investigated by computational modeling. Importantly, for all the four NASTs the interdigitated bilayer arrangement was consistently observed in the computational models with higher energies also at least up to the 4th lowest energy model. This strongly supports the interpretation drawn from the PXRD studies that the NASTs pack in an interdigitated fashion in the solid state.

Although the above results suggested that all the four NASTs investigated by computational modeling form interdigitated structures in the solid state, considerable variation was seen in the orientation of the serotonin moiety in the head group region as well as in the acyl chain tilt among the various NASTs and also between the different low energy structures of each NAST. Therefore, we would like to limit our interpretation of the modeling results only to indicate that the acyl chain packing in the NASTs is interdigitated.

Table 3
Lamellar *d*-spacings of NASTs with different acyl chain lengths ($n = 11$–20), derived from the powder X-ray diffraction data.

Chain length (n)	Average *d*-spacing (d_{avg})
11	22.5 ± 0.4
12	22.8 ± 0.4
13	23.8 ± 0.4
14	25.1 ± 0.6
15	26.3 ± 0.5
16	26.7 ± 0.2
17	27.9 ± 0.3
18	28.8 ± 0.3
19	30.9 ± 0.4
20	31.2 ± 0.3

3.9. Interaction of N-myristoylserotonin with DMPC

N-Acylserotonins are endogenous fatty amides present in the gastrointestinal tract of mammals. Since cell membranes contain a variety of lipids such as phospholipids, sphingolipids and sterols, it is of interest to investigate the interaction of NASTs with other membrane lipids. In view of this, in the present study, we have investigated the effect of incorporating *N*-myristoylserotonin (NMST) in DMPC membranes by DSC. Fig. 8A shows DSC thermograms of hydrated DMPC membranes in the absence and in the presence of different mol fractions of NMST. The thermogram of DMPC alone shows a pretransition at 13.3 °C and a main transition at 23.8 °C, which are consistent with literature values [27]. The pretransition corresponds to the transformation of tilted gel phase to ripple gel phase ($L_{\beta'} \rightarrow P_{\beta'}$) whereas the main transition corresponds to the gel–liquid crystalline phase transition ($P_{\beta'} \rightarrow L_{\alpha}$) [38]. At low mole fractions (up to 5 mol%), addition of NMST did not significantly alter either the pretransition or the main chain-melting phase transition of DMPC. At higher mol fractions (up to 30 mol%) of NMST, the pretransition peak becomes sharper with increase in the phase transition temperature, whereas the main transition shifts to lower temperatures (Fig. 8B). While the enthalpy of the pretransition does not exhibit much variance and remains nearly

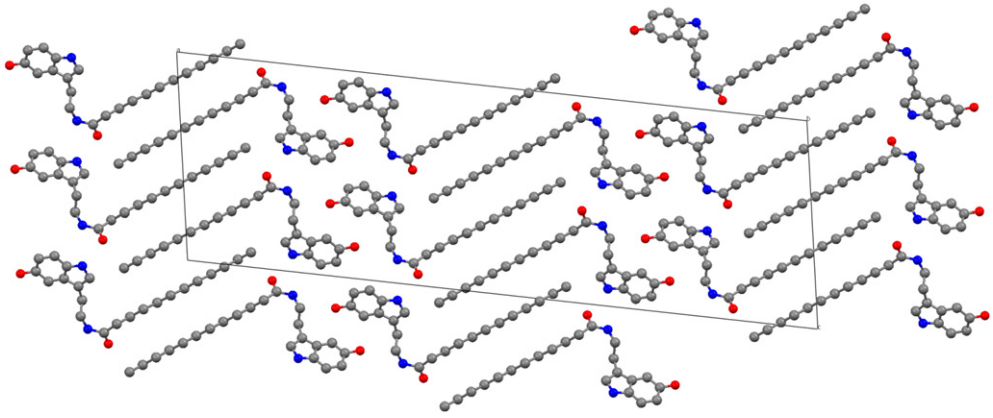

Fig. 7. Molecular packing of NLST viewed down the *b*-axis. Hydrogen atoms were omitted for clarity. Color code: red, oxygen; blue, nitrogen; grey, carbon.

constant up to 40 mol% NMST, enthalpy of the main transition exhibits a distinct increase when the content of NMST in the mixture is increased up to 5 mol%, but decreases steadily thereafter (Fig. 8C). Values of transition temperatures, enthalpies and entropies obtained from the DSC thermograms shown in Fig. 8 are given in Table S6. These results suggest that incorporation of NMST stabilizes the tilted gel phase ($L_{\beta'}$) of DMPC but destabilizes the ripple phase ($P_{\beta'}$) above 5 mol%. Hydrogen bonding between the hydroxyl group of the serotonin moiety with either the ester carbonyls or the phosphodiester group could possibly play a role in the stabilization of the gel phase. Based on X-ray and neutron diffraction studies on lecithin–cholesterol bilayers and changes induced by cholesterol in the ^{13}C NMR chemical shift of the phospholipid carbonyl resonance, such hydrogen bonding was proposed to exist between the 3-β hydroxyl of cholesterol and the *sn*-2 carbonyl group of phosphatidylcholines [39,40].

An important consequence of incorporating NASTs into phosphatidylcholine membranes would be its influence on the permeability of the vesicles. For example, it has been shown that incorporation of cholesterol into DMPC vesicles progressively reduces the leakage of carboxyfluorescein (CF) up to 30 mol% sterol [41], whereas *N*-dodecanoyl derivatives of amino acids such as glycine, valine, leucine and phenylalanine did not alter the permeability at low concentrations but led to complete leakage at concentrations close to their critical micellar concentrations [42]. The effect of incorporating NASTs on the permeability of phosphatidylcholine membranes can be assessed by monitoring the kinetics of the leakage of fluorescent probes such as CF or riboflavin that is loaded inside the vesicles [43,44]. Such studies are currently underway in our laboratory.

4. Conclusions

In the present study a homologous series of saturated *N*-acylserotonins with varying acyl chain lengths ($n = 11$–20) have been synthesized and their physicochemical properties were investigated by biophysical approaches. Differential scanning calorimetric studies showed that in the dry and hydrated states the transition temperatures, transition enthalpies and transition entropies of NASTs exhibit odd–even alternation with the values of the even chain length series being slightly higher. In both dry and hydrated states NASTs with odd and even chain lengths independently display linear dependence of the transition enthalpies and transition entropies on the chain length. These results suggest that the packing and intermolecular interactions between NAST molecules are likely to be very similar in the entire chain length series. Results of powder X-ray diffraction and computational modeling studies suggest that the acyl chains in NASTs are packed in an interdigitated fashion. DSC studies indicate that *N*-myristoylserotonin mixes reasonably well up to 30 mol% in dimyristoylphosphatidylcholine and stabilizes the tilted gel phase of the latter. These results provide a

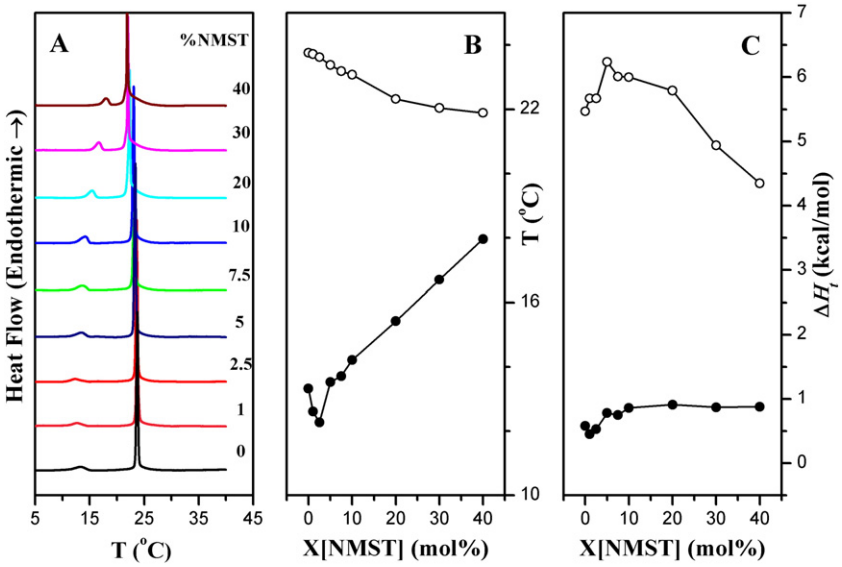

Fig. 8. DSC studies on the interaction of NMST with DMPC membranes. A) Thermograms of DMPC/NMST mixtures, B) Transition temperatures of main transition (O) and pretransition (●), and C) enthalpies of main transition (O) and pretransition (●).

thermodynamic basis for understanding the functional roles of NASTs in their parent tissues.

Acknowledgements

This work was supported by a research grant from the Department of Science and Technology (India) to MJS. STR was supported by a Senior Research Fellowship from the Council of Scientific and Industrial Research (India). The University Grants Commission (India) is acknowledged for their support through the UPE and CAS programs, to the University of Hyderabad and School of Chemistry, respectively.

Appendix A. Supplementary data

Six tables (S1–S6) and six figures (S1–S6) are given as Supporting Information. Supplementary data associated with this article can be found, in the online version, at http://dx.doi.org/10.1016/j.bbamem.2014.09.012.

References

[1] S. Spiegel, D. Foster, R. Kolesnickz, Signal transduction through lipid second messengers, Curr. Opin. Cell Biol. 8 (1996) 159–167.
[2] A.Z. Fernandis, M.R. Wenk, Membrane lipids as signaling molecules, Curr. Opin. Lipidol. 18 (2007) 121–128.
[3] G.D. Paolo, T.-W. Kim, Linking lipids to Alzheimer's disease: cholesterol and beyond, Nature 12 (2011) 284–296.
[4] C.R. Santos, A. Schulze, Lipid metabolism in cancer, FEBS J. 279 (2012) 2610–2923.
[5] D. Cotter, A. Maer, C. Guda, B. Saunders, S. Subramaniam, LMPD: LIPID MAPS Proteome database, Nucleic Acids Res. 34 (2006) D507–D510.
[6] E. Fahy, M. Sud, D. Cotter, S. Subramaniam, LIPID MAPS online tools for lipid research, Nucleic Acids Res. 35 (2007) W606–W612.
[7] http://www.lipidmaps.org/data/structure/index.html.
[8] C. Ezzili, K. Otrubova, D.L. Boger, Fatty acid amide signaling molecules, Bioorg. Med. Chem. Lett. 20 (2010) 5959–5968.
[9] H.H.O. Schmid, P.C. Schmid, V. Natarajan, *N*-Acylated glycerophospholipids and their derivatives, Prog. Lipid Res. 29 (1990) 1–43.
[10] K.D. Chapman, Occurrence, metabolism, and prospective functions of *N*-acylethanolamines in plants, Prog. Lipid Res. 43 (2004) 302–327.
[11] M.J. Swamy, P.K. Tarafdar, R.K. Kamlekar, Structure, phase behaviour and membrane interactions of *N*-acylethanolamines and *N*-acylphosphatidylethanolamines, Chem. Phys. Lipids 163 (2010) 266–279.
[12] M. Connor, C.W. Vaughn, R.J. Vandenberg, *N*-Acyl amino acids and *N*-acyl neurotransmitter conjugates: neuromodulators and probes for new drug targets, Br. J. Pharmacol. 160 (2010) 1857–1871.
[13] K.C.M. Verhoeckx, T. Voortman, M.G.J. Balvers, H.F.J. Hendriks, H.M. Wortelboer, R.F. Witkamp, Presence, formation and putative biological activities of *N*-acyl serotonins, a novel class of fatty-acid derived mediators, in the intestinal tract, Biochim. Biophys. Acta 1811 (2011) 578–586.
[14] M. Berger, J.A. Gray, B.L. Roth, The expanded biology of serotonin, Annu. Rev. Med. 60 (2009) 355–366.
[15] T.J. Pucadyil, S. Kalipatnapu, A. Chattopadhyay, The serotonin$_{1A}$ receptor: a representative member of serotonin receptor family, Cell. Mol. Neurobiol. 25 (2005) 553–580.
[16] Y.D. Paila, A. Chattopadhyay, The human serotonin receptor expressed in neuronal cells: toward a native environment for neuronal receptors, Cell. Mol. Neurobiol. 26 (2006) 925–942.
[17] P.P. Bertrand, R.L. Bertrand, Serotonin release and uptake in the gastrointestinal tract, Auton. Neurosci. 153 (2010) 47–57.
[18] M.D. Gershon, J. Tack, The serotonin signaling system: from basic understanding to drug development for functional GI disorders, Gastroenterology 132 (2007) 397–414.
[19] A. Sikander, S.V. Rana, K.K. Prasad, Role of serotonin in gastrointestinal motility and irritable bowel syndrome, Clin. Chim. Acta 403 (2009) 47–55.
[20] P.G. McLean, R.A. Borman, K. Lee, 5-HT in the enteric nervous system: gut function and neuropharmacology, Trends Neurosci. 30 (2007) 9–13.
[21] T. Bisogno, D. Melck, L. De Petrocellis, M.Yu. Bobrov, N.M. Gretskaya, V.V. Bezuglov, N. Sitachitta, W.H. Gerwick, V.D. Marzo, Arachidonylserotonin and other novel inhibitors of fatty acid amide hydrolase, Biochem. Biophys. Res. Commun. 248 (1998) 515–522.
[22] S. Maione, L. De Petrocellis, V. de Novellis, A.S. Moriello, S. Petrosino, E. Palazzo, F.S. Rossi, D.F. Woodward, V. Di Marzo, Analgesic actions of *N*-arachidonoyl-serotonin, a fatty acid amide hydrolase inhibitor with antagonistic activity at vanilloid TRPV1 receptors, Br. J. Pharmacol. 150 (2007) 766–781.
[23] V. Micale, L. Cristino, A. Tamburella, S. Petrosino, G.M. Leggio, F. Drago, Anxiolytic effects in mice of a dual blocker of fatty acid amide hydrolase and transient receptor potential vanilloid type-1 channels, Neuropsychopharmacology 34 (2009) 593–606.
[24] C.S. John, P.J. Currie, *N*-Arachidonoyl-serotonin in the basolateral amygdala increases anxiolytic behavior in the elevated plus maze, Behav. Brain Res. 233 (2012) 382–388.
[25] G. Ortar, M.G. Cascio, L. De Petrocellis, E. Morera, F. Rossi, A. Schiano-Moriello, M. Nalli, V. de Novellis, D.F. Woodward, S. Maione, V.D. Marzo, New *N*-arachidonoylserotonin analogues with potential "dual" mechanism of action against pain, J. Med. Chem. 50 (2007) 6554–6569.
[26] S.T. Reddy, P.K. Tarafdar, R.K. Kamlekar, M.J. Swamy, Structure and thermotropic phase behavior of a homologous series of bioactive *N*-acyldopamines, J. Phys. Chem. B 117 (2013) 8747–8757.
[27] D. Marsh, Handbook of Lipid Bilayers, CRC Press, Boca Raton, FL, 1990.
[28] M.J. Frisch, G.W. Trucks, H.B. Schlegel, G.E. Scuseria, M.A. Robb, J.R. Cheeseman, J.A. Montgomery Jr., T. Vreven, K.N. Kudin, J.C. Burant, J.M. Millam, S.S. Iyengar, J. Tomasi, V. Barone, B. Mennucci, M. Cossi, G. Scalmani, N. Rega, G.A. Petersson, H. Nakatsuji, M. Hada, M. Ehara, K. Toyota, R. Fukuda, J. Hasegawa, M. Ishida, T. Nakajima, Y. Honda, O. Kitao, H. Nakai, M. Klene, X. Li, J.E. Knox, H.P. Hratchian, J.B. Cross, V. Bakken, C. Adamo, J. Jaramillo, R. Gomperts, R.E. Stratmann, O. Yazyev, A.J. Austin, R. Cammi, C. Pomelli, J.W. Ochterski, P.Y. Ayala, K. Morokuma, G.A. Voth, P. Salvador, J.J. Dannenberg, V.G. Zakrzewski, S. Dapprich, A.D. Daniels, M.C. Strain, O. Farkas, D.K. Malick, A.D. Rabuck, K. Raghavachari, J.B. Foresman, J.V. Ortiz, Q. Cui, A.G. Baboul, S. Clifford, J. Cioslowski, B.B. Stefanov, G. Liu, A. Liashenko, P. Piskorz, I. Komaromi, R.L. Martin, D.J. Fox, T. Keith, M.A. Al-Laham, C.Y. Peng, A. Nanayakkara, M. Challacombe, P.M.W. Gill, B. Johnson, W. Chen, M.W. Wong, C. Gonzalez, J.A. Pople, Gaussian 03, Revision C.02, Gaussian, Inc., Wallingford CT, 2004.
[29] Materials Studio, 6.0 V, Accelrys Inc., San Diego, CA, 2010.
[30] K. Larsson, Physical properties—structural and physical characteristics, in: F.D. Gunstone, J.L. Harwood, F.B. Padley (Eds.), The Lipid Handbook, Chapman and Hall, London, 1986, pp. 321–384.
[31] R.K. Kamlekar, P.K. Tarafdar, M.J. Swamy, Synthesis, calorimetric studies and crystal structures of diacylethanolamines with matched chains, J. Lipid Res. 51 (2010) 42–52.
[32] D. Marsh, M.J. Swamy, Derivatized lipids in membranes: physico-chemical aspects of *N*-biotinyl phosphatidylethanolamines, *N*-acyl phosphatidylethanolamines and *N*-acylethanolamines, Chem. Phys. Lipids 105 (2000) 43–69.
[33] P.K. Tarafdar, S.T. Reddy, M.J. Swamy, Nonclassical odd–even alternation in mixed-chain diacylethanolamines: implications of polymorphism, Cryst. Growth Des. 12 (2012) 1132–1140.
[34] M. Ramakrishnan, M.J. Swamy, Differential scanning calorimetric studies on the thermotropic phase transitions of *N*-acylethanolamines of odd chain lengths, Chem. Phys. Lipids 94 (1998) 43–51.
[35] T. Head-Gordon, Is water structure around hydrophobic groups clathrate-like? Proc. Natl. Acad. Sci. U. S. A. 92 (1995) 8308–8312.
[36] D. Marsh, Biomembranes, Supramolecular Structure and Function, in: G. Pifat, J.N. Herak (Eds.), Plenum Press, New York, 1982, pp. 127–178.
[37] D.M. Small, Lateral chain packing in lipids and membranes, J. Lipid Res. 25 (1984) 1490–1500.
[38] S. Ali, S. Minchey, A. Jonaff, E. Mayhew, A differential scanning calorimetry study of phosphocholines mixed with paclitaxel and its bromoacylated taxanes, Biophys. J. 78 (2000) 246–256.
[39] N.P. Franks, W.R. Lieb, The structure of lipid bilayers and the effects of general anaesthetics. An X-ray and neutron diffraction study, J. Mol. Biol. 133 (1979) 469–500.
[40] M.B. Sankaram, T.E. Thompson, Cholesterol-induced fluid-phase immiscibility in membranes, Proc. Natl. Acad. Sci. U. S. A. 88 (1991) 8686–8690.
[41] S. Bhattacharya, S. Haldar, Interactions between cholesterol and lipids in bilayer membranes. Role of lipid headgroup and hydrocarbon chain-backbone linkage, Biochim. Biophys. Acta 1467 (2000) 39–53.
[42] A. Ohta, Y. Miyazato, H. Sasaki, K. Yasuhara, T. Asakawa, Effect of functional groups on incorporation behavior of amino acid-type surfactant into phospholipid vesicle membrane, J. Oleo Sci. 58 (2009) 609–615.
[43] S. Bhattacharya, S. Haldar, Synthesis, thermotropic behavior, and permeability properties of vesicular membranes composed of cationic mixed-chain surfactants, Langmuir 11 (1995) 4748–4757.
[44] E. Haba, A. Pinazo, R. Pons, L. Pérez, A. Manresa, Complex rhamnolipid mixture characterization and its influence on DPPC bilayer organization, Biochim. Biophys. Acta 1838 (2014) 776–783.